

HIGH-ENERGY-DENSITY FUEL BLENDING STRATEGIES AND DROP DISPERSION FOR FUEL COST REDUCTION AND SOOT PROPENSITY CONTROL

J. Bellan and K. Harstad

Jet Propulsion Laboratory, California Institute of Technology, Pasadena, CA. 91109

Word Count: 5658 (197 lines x 14 words; table, 200; figures, 200+ 10x 250)

Colloquium: Internal Combustion Engines and Spray Combustion

Corresponding author:

Dr. J. Bellan

Jet Propulsion Laboratory

California Institute of Technology

MS. 125-121

4800 Oak Grove Drive

Pasadena, CA 91109

USA

Tel: (81 8) 354-6959

Fax: (818) 393-1633

Email: Josette.Bellan@jpl.nasa.gov

ABSTRACT

The idea that low soot propensity of high-energy-density (HED) liquid sooting fuels and cost reduction of a multicomponent energetic fuel can be achieved by doping a less expensive, less sooting liquid fuel with HED is tested through numerical simulations. The model represents an axisymmetric, polydisperse, dense cluster of binary-fuel (solvent/solute) spherical drops embedded into a vortex. The partial density of the evaporated fuels which is symptomatic of sooting propensity is compared for uncharged and electrostatically charged drops; charging is here used as an effective way to increase dispersion and reduce sooting propensity. Results from the simulations show that while the solvent soot propensity indeed decreases with drop charging, contrary to simplistic expectations, addition of HED a. a solute increases sooting propensity of the solute with increased drop dispersion. This is due to the additional dispersion maintaining the slip velocity at the drop surface and preferentially evaporating the solute. These counterintuitive but correct physical effects are independent of the initial solvent/solute mass ratio and decrease with decreasing solute volatility. Based upon these results, blending strategies are suggested for minimizing sooting propensity and decreasing fuel costs.

1. INTRODUCTION

High-energy-density (HED) fuels developed over the last decades to replace conventional liquid fuels have the drawback of high soot propensity which makes them environmentally and strategically unacceptable. Experimental evidence of heavy sooting from such fuels has been presented by Law[1]. Soot propensity is defined here as the ability of a fuel to form soot precursors through nucleation reactions; it does not refer to soot growth, or soot production which includes the additional effect of soot destruction through oxidation reactions.

To reduce soot propensity one has at least two options: (1) drop dispersion (experimentally investigated by Sangiovanni and Liscinsky[2]) to avoid the crest ion of fuel-rich-vapor regions where soot nucleation occurs, and (2) fuel blending. Bellan and Harstad [3] have shown that electrostatically induced dispersion does indeed reduce soot propensity; electrostatic dispersion has also been found superior to mechanical dispersion [4]. Here we examine the possibilities of: (1) deriving a fuel blending strategy that can reduce both the cost of fuel (HED fuels are expensive) and the sooting propensity, and (2) combining fuel blending and drop dispersion to further reduce soot propensity. We focus this study on binary fuels as they are the simplest multi component fuels.

2. MODEL

The configuration studied is that of an axisymmetric (coordinates r -, θ , z), polydisperse, dense cluster of spherical evaporating drops embedded into an axisymmetric vortex. Due to the centrifugal motion of the vortex, the drop cluster quickly forms an inner boundary additionally to its existing outer boundary. The model has been described in detail by Harstad and Bellan [5] and will be only briefly summarized here. The mathematical formulation consists of two fully (two-way) coupled sets of equations: one for the gas and the other for the drops. The gas is followed in an Eulerian way whereas the drops are followed by initial size class in a Lagrangian way. Each drop initial size class evolves into a multitude of drop sizes as the drops evaporate at different rates according to their location within the cluster. The set of equations for the gas contains the continuity equation, the inviscid momentum equation (radial and azimuthal velocities), species conservation equations, the energy equation and the equation of state. We define statistically a sphere of influence around

each drop so that the ensemble of the spheres of influence and the interstitial space constitute the cluster volume. The drops conservation equations are the drop number conservation, momentum conservation (radial and azimuthal velocities) and the quasi-steady energy and species equations for each drop in its sphere of influence; the boundary conditions at the edge of each sphere of influence are given by the values of the gas dependent variables. Coupling between drops and gas occurs through heat transfer, evaporation (mass transfer), and momentum transfer. Heat transfer is modeled in each sphere of influence and yields an analytic expression for the temperature profile in the sphere of influence; since $Le_g \approx 1$, the mass fraction profiles are found by similarity from the temperature profile. Evaporation is described by the Langmuir-Knudsen non-equilibrium kinetic law since the drops are small ($R^0 \leq 2.5 \times 10^{-3} \text{ cm}$; R is the drop radius) and the initial gas temperature is much larger than the boiling point of the fuels [6]. Momentum transfer occurs through form drag on the drops and through blowing of mass from the drops; the drag coefficient contains a correction accounting for mass blowing and the drag term is function of the drop number density. Thus, source terms appear in the gas continuity equation, both gas and drop momentum equations and the gas energy equation. Gas turbulence is modeled using the Prandtl mixing length hypothesis where small scale turbulence resulting from drops differential azimuthal velocity is modeled by similarity with the Stokes-Einstein relationship, except that here instead of the motion being induced by thermal fluctuations, it is induced by the fluctuations of the small scale turbulent eddies. When the drops are charged, there is an additional electrostatic radial force in the momentum equations as described in detail by Bellan and Harstad [3].

The internal drop model for drop heating and solvent/solute evaporation is that of Harstad and Bellan [7]. The two main assumptions of the model is that the solute is much more volatile than the solvent (once at the drop surface, the solute evaporates immediately) and that the mass fraction of solute is smaller by almost an order of magnitude than that of the solvent. In general, the evaporation rate is the sum of three terms: the evaporation rate of the solvent according to the Langmuir-Knudsen (L-K) evaporation law, the diffusion rate of the solute through the boundary layer and the rate of surface layer stripping of the drop. However, two important limiting regimes of evaporation are identified according to the value of a dimensionless number, $Be \equiv -[R/(D_m u_i)]^{0.5} (dR/dt)$, that represents the ratio of the mass regression rate

to a characteristic volatile diffusion rate; D_m is the liquid mass diffusivity, u_l is the velocity of the liquid inside the drop and t is the time. When $Be \ll 1$, diffusion into the boundary layer governs the rate of species transfer from the liquid core to the drop surface; subsequent mass transfer from the drop surface to the gas phase is governed by evaporation according to the I-K evaporation law. These are sequential processes and the overall mass transfer is determined by the lower of the diffusion and evaporation rates. In contrast, when $Be \gg 1$, transfer of the solute to the gas phase is governed by the rate of surface layer stripping (the evaporation rate of the drop). Because surface layer stripping and diffusion rate from the core to the boundary layer are competitive processes, the overall transfer of solute from the core to the gas is governed by the higher of the diffusion and drop regression rates. The quasi-steady boundary layer assumption is consistent with $Be \ll 1$ but inconsistent with $Be \gg 1$.

3. SIMULATIONS RATIONALE

Early experiments with cubane by Law [1] pointed out one of the main drawbacks of cubane as a liquid propulsion fuel: in solution with other fuels it does not participate in combustion and instead it accumulates in the fuel creating an increasingly viscous, less volatile mixture until supersaturation occurs when a temperature larger than the boiling point of the more volatile fuel is attained. It is only at that time that microexplosions ensue and cubane participates in the burning process. To palliate this aspect of cubane, liquid cubane compounds were synthesized and studied. For example, experiments by Law [8] at $p = 0.25$ atm showed that methylcubane (MTCU) has a considerably larger burning rate constant, K , than nonane (NONA), a typical hydrocarbon; experiments were also performed with pure nonane and pure MTCU showing the increase in K with p , and with mixtures of nonane/MTCU. The rationale of using mixtures of a HED fuel and a typical hydrocarbon is that HED fuels are expensive and thus might not be economically feasible to use; judiciously used in solution with a hydrocarbon they might still enhance burning, yet be more economical.

Taking guidance from the experiments of Law [8], MTCU was chosen as a typical HED to be used as a solute in a mixture with a hydrocarbon. Following methods previously outlined [9], the properties of MTCU were estimated as seen in Table 1. To validate the calculated properties of MTCU, simulations were

performed with a very dilute cluster of uniformly-distributed, monodisperse drops of 0.438 μm diameter at 0.13 atm and of 0.531 μm diameter at 0.25 atm (the conditions in the experiment of Law [8]) in a vortex embedded into a very hot T environment (3000 K) to duplicate the high flame temperature of MTCU (which however had not been measured [8]). The cluster radius was 2 cm; both the vortex and the drops had negligible velocities [$0(10^{-3})$ cm] to duplicate the convection-free environment of the experiment. The calculations at 0.13 atm yielded $K = 1.125 \text{ mm}^2/\text{s}$ which should be compared to the experimental value of $1.2 \text{ mm}^2/\text{s}$. Calculations at the higher pressure (0.25 atm) could not be completed due to convergence problems as the model and code have not been derived for the very dilute regime.

Plots of the saturation pressure versus the temperature for benzvalene (BV), quadricyclane (QUAD), dihydrobenzvalene (DHBV), MTCU, heptane (HPT) and NONA appear in Fig. 1 (properties of BV, QUAD and DHBV were given elsewhere [3]). These plots show that the difference in volatility between MTCU and NONA is such that for Law's experimental conditions of $p = 0.13$ atm and 0.25 atm, MTCU is more volatile than NONA and thus the mixture NONA/MTCU is indeed a reasonable solvent/solute mixture. However, for $p > 1$ atm, it is NONA that is more volatile than MTCU and the entire concept of the HED being used as a solute breaks down. Moreover, it appears that for $p > 1$ atm MTCU is the least volatile of the substances considered here and thus it cannot serve as a solute in any combination with them. Further examination of Fig. 1 shows that NONA is considerably less volatile than BV, QUAD or DHBV and thus can represent the solvent for which the other three fuels can be solutes.

4. RESULTS

The results of the calculations were used to examine the evolution of the partial density of fuel, solvent and solute, for both uncharged and charged clusters of drops, and to determine the influence of the solvent/solute mass fraction and solute volatility upon the results. The simulations were performed with a binary initial size distribution ($R_1^0 = 2 \times 10^{-3} \text{ cm}$, $R_2^0 = 2.5 \times 10^{-3} \text{ cm}$), an initial cluster radius of 2 cm, initial drop and far field gas temperature, $T_{g\infty}^0$, of 300 K and 600 K respectively, $p = 1 \text{ atm}$, null initial drop radial velocity, irrotational gas tangential velocity ($100/r \text{ cm/s}$) and tangential drop velocity of the form $(75/r + 200r) \text{ cm/s}$; the initial gas radial velocity is found by solving the energy equation. The far field gas temperature

is a function of time, $T_{g\infty}^0 [1 + t/(6 \times 10^{-3})]$, to simulate the passage of the vortex through an increasing temperature region. The functional form of the drop number density distribution is given in [3], the air/fuel mass ratio is 0.314 and the ratio of the initial maximum drop number distributions is 1/3 with the smaller drops being more numerous. The drop number density distribution is such that except at the cluster boundaries, the nondimensional radius of the sphere of influence is in that dense regime [7]. Calculations with charged drops are stopped for any drop when its Rayleigh limit is encountered [3]. For the present initial conditions, the Rayleigh limit occurs typically when the drops reach 5% of their initial radius; as a result, the limit occurs first at the outer cluster boundary [5]. Any outer-boundary drop that has reached the limit is further neglected because its mass, momentum, energy and charge do not affect the other drops. However, inner boundary drops evaporate almost as fast as outer boundary drops [5]; when an inner boundary drop has reached the Rayleigh limit, the entire calculation is stopped since the cluster can no longer remain an entity.

4.1. General behavior

As shown previously [3], when single-component drops are charged, the partial gaseous fuel density decreases due to increased drop dispersion, thereby reducing soot propensity.

Figures 2-5 contain results from simulations made with NONA/DHBV, the initial mass ratio being 80/20. The plots are made for the dependent variables related to drops in initial-size-class-1; they are qualitatively representative of initial-size-class-2 as well. Instead of plotting the variables versus the radial location in the cluster, r , the abscissa in Figs. 2-5 is the residual drop radius, R_i/R_1^0 , and the variable parameter along each curve is r ; the multivalued character of the curves arises from the fact that there are several locations within the cluster at which the residual drop radius is the same. The advantage of plots versus R_i/R_1^0 is that they indicate the importance of an effect during the drops lifetime; for example, when the residual radius is 0.3, less than 3% of the mass is left in the drops.

Initially the drops evaporate in the liquid mass diffusion controlled mode ($Be \ll 1$, see Fig. 2), but gradually the surface layer stripping (frozen composition) mode ($Be \gg 1$) takes over; however, it appears the last mode does not occur until the drops are almost entirely evaporated. The large initial slip velocity

[(difference between drops and gas velocity); Fig. 2] creates shear at the drops surface and induces a circulatory motion inside the drops which enhances liquid mass diffusion (an otherwise slow process with a characteristic time larger than the drop lifetime) and preferentially brings the solute to the surface. As drag reduces the slip velocity, the circulatory motion decreases and liquid mass diffusion is no longer effective as clearly indicated in Fig. 2. Plots of the solute evaporation rate fraction, \dot{m}_{solute}/\dot{m} , and of the solute mass fraction in the drop core, $Y_{solute,dc}$, also found in Fig. 2 show consistently with the above interpretation that the initially large evaporation fraction, 0.6, quickly decreases to ~ 0.1 and remains small resulting in the composition of the drop core changing from 80/20 to about 84/16 and remaining frozen. This means that in fact Be does not have to be $\gg 1$ for the liquid mass diffusion mode to cease; $Be \simeq 0(10)$ suffices. This transition from the first to the second evaporation mode occurs when there is about 50% of the mass left in the drops.

Similar plots to those of Fig. 2 appear in Fig. 3 for the identical initial conditions except the drops are charged with 25% of the maximum charge [3]. The effect of charging is to maintain the slip velocity, and thus to keep Be small; the drop thus continues to evaporate in the liquid mass diffusion mode resulting in the solute being continuously depleted from the drop core and the solute evaporation rate fraction continuously decreasing.

A comparison of the gaseous mass fractions of solvent and solute for the uncharged and charged cases is shown in Fig.4. The effect of charging is to reduce the gas solvent mass fraction and to increase the gas solute mass fraction. The larger solute mass fraction results from preferential evaporation maintained by the large slip velocity. In fact, any means of drop dispersion (not only charging) will have the same effect. However, it is not the mass fractions, but the partial gas densities that indicate soot propensity; they are plotted for comparison in Fig. 5. The comparison shows the dramatic reduction in the solvent partial density due to reductions in both density and mass fraction [3], and the increase in the solute partial density as the reduction in the total density cannot compensate for the larger solute mass fraction. This means that if the solute is the more potentially sooting component, the sooting propensity of the fuel has not been decreased, and perhaps has even been increased. A preliminary conclusion is that soot reduction strategies for pure fuels cannot automatically be translated to fuel blends.

4.2. Effect of the initial composition

To investigate the effect of the initial composition, simulations have been performed for 90/10 and 95/5 liquid mass compositions with the same fuel and initial conditions; the small % of solute reflects one of the assumptions of the binary-fuel model [7]. The results (not illustrated) were essentially the same: increasing dispersion decreases the solvent, but not the solute, partial density.

4.3. Effect of the solute relative volatility with respect to solvent

According to Fig. 1, BV is slightly less volatile than DHBV, whereas QUAD is considerably less volatile than DHBV at $p = 1atm$. Simulations were therefore performed with NONA/BV and NONA/QUAD for identical initial conditions to those in the NONA/DHBV simulations to determine the effect of volatility upon soot propensity reduction through enhanced dispersion.

A small decrease in solute relative volatility (BV vs DHBV) does not influence the solvent partial density reduction but renders the relative solute soot propensity a function of time: initially the solute partial density of charged drops is larger, but a tapering off effect renders it almost equal to that of uncharged drops at the Rayleigh limit (not shown). A larger reduction in the solvent relative volatility (NONA/QUAD, Fig. 6) accentuates the trend: the initial partial density of the solute is only slightly larger when the drops are charged and quickly becomes equal to that in the uncharged case. The physical explanation is not in the extent of preferential evaporation as a function of the relative solvent/solute volatility since it is always small; it is an indirect effect through the modification of the latent heat of the mixture. Thus, if HED fuels are blended with other fuels of similar volatility (in the range of combustion device operation), the behavior of the blend will become closer to that of a single-component fuel and drop dispersion will be effective in reducing soot propensity.

5. CONCLUSIONS

Simulations of polydisperse, dense clusters of drops evaporating in a vortex were performed for several binary-fuel combinations with the solute being a high-energy-density fuel. Both uncharged and charged drops were considered; the simulations with charged drops were ended when the Rayleigh limit was reached

at the inner cluster boundary. Drop charging was used because it was previously shown to be an effective way for dispersing drops and reducing soot propensity.

The results show that increased drop dispersion results in the solute evaporating preferentially for longer times. This increases the gaseous mass fraction of the solute and despite the reduction in total density increases the partial density of the solute, The expected consequence is that if the solute is the more sooting component of the blend, soot propensity might actually increase instead of decreasing. These conclusions are independent of the initial liquid composition within the limits of the solvent/solute assumption. The results also show that as the solvent/solute volatility ratio increases towards unity, preferential evaporation of the solute decreases and the blend acts more like a single-component fuel.

The above results show that soot reduction strategies for single-component fuels are not necessarily extendable to fuel blends. These results also indicate that there might be two HE D-fuel blending strategies for fuel cost and soot propensity reduction. The first strategy is blending the HED with a fuel of same volatility at the operating conditions; the HED can be the solute and thus the cost of the blend will be relatively low. The second strategy is blending the HED with a higher volatility fuel (the HED is now the solvent); this will still reduce the fuel cost with respect to a single-component HED, and will insure that soot propensity is decreased with increasing drop dispersion since the HED is now the solvent.

Acknowledgment

This research was carried out at the Jet Propulsion Laboratory, California Institute of Technology, under a contract with the National Aeronautics and Space Administration (NASA), and under sponsorship from the Office of Naval Research , with Dr. Gabriel Roy as technical monitor through an interagency agreement with NASA.

References

- [1] Law, C. K., "Combustion Studies of Energetic Liquid Materials", *Proc. 7th ONR Propulsion Meeting*, p.110, 1994
- [2] Sangiovanni, J. J. and Liscinsky, D. S., *20th Symp.(Int.) on Combustion*, p. 1063, 1984
- [3] Bellan, J. and Harstad, K., *26th Symp. (Int.) on Combustion*, pp. 1713-1722, 1996
- [4] Bellan, J. and Harstad, K., "Dispersion (Electrostatic/Mechanical) and Fuel Properties Effects on Soot Propensity", submitted to *Atomization and Sprays*, 1997
- [5] Harstad, K. and Bellan, J., *Int. J. Multiphase Flow*, 23(5), pp. 899-925, 1997
- [6] Miller, R. S., Harstad, K. G. and Bellan, J., "Evaluation of Equilibrium and Non-Equilibrium Evaporation Models for Many-Droplet Gas-Liquid Flow Simulations", submitted to *Int. J. Multiphase Flows*, 1997
- [7] Harstad, K. and Bellan, J., *Atomization and Sprays*, 1, pp.367-388, 1991
- [8] Law, C. K., Sung, C. J., Wang, H. and Zhu, D. L., "Combustion Studies of Energetic Liquid Materials", *Proc. 8th ONR Propulsion Meeting*, p. 192, 1995
- [9] Bellan, J., "Electrostatic Dispersion and Evaporation of Dense and Dilute Clusters of Drops of High-Energy Fuel for Soot Control", *Proc. 8th ONR Propulsion Meeting*, p.168-182, 1995

Symbol	HPT	NONA	MTCU
$\Phi_s \equiv (\text{air/fuel}) \text{ mass}$	15.1	15	13.4
w, g/mole	100.2	128.26	118
T_{bn} , K	371.6	424	423
L_{bn} , cal/g	64.16	78.98	58.1
ΔC_p , cal/(gK)	-9.08 x10-3	-7.57 X1 0-3	0(assm)
ρ_l , g/cm ³	0.684	0.718	0.908
C_{pl} , cal/(gK)	0.539	0.22	0.2
μ_l , g/(cms)	0.208 x10-2	0.661 x10 ⁻² (assm)	0.35x10 ⁻² (assm)
$D_{ml}(Le_l=10)$, cm ² /s	-	1.353 X1 0-4	1.27 x 10 ⁻⁴
λ_l , cal/(gK)	2.406 x10-4	2.525 x10-4	2.44 x10-4
$C_{pg}(T_g = 424 \text{ K})$	0.528	0.527	0.4

1 .Properties of fuels

Figure Captions

Figure 1. Saturation pressure versus temperature for BV (—), QUAD (----), DHBV (- · - · -), MTCU (· · · · ·), HPT (— —), NONA (- · - · - · -).

Figure 2. Slip velocity and Be (a), relative solute evaporation rate and solute liquid mass fraction in the drop core (b) versus the residual drop radius for initial-size-class-1. Uncharged drops of NONA (80%)/DHBV(20%). Curves are for different times as follows: 6.8×10^{-5} s (· · · · ·), 1.4×10^{-3} s (—), 2.8×10^{-3} s (- - -), 4.2×10^{-3} s (- · - · -), 5.5×10^{-3} s (— —), 6.2×10^{-3} s (- · · · · ·), 1.2×10^{-2} s (—o—).

Figure 3. Slip velocity and Be (a), relative solute evaporation rate and solute liquid mass fraction in the drop core (b) versus the residual drop radius for initial-size-class-1. Charged drops of NONA (80%)/DHBV(20%). Curves are for different times as follows: 6.8×10^{-5} s (· · · · ·), 1.4×10^{-3} s (—), 2.8×10^{-3} s (- - -), 4.2×10^{-3} s (- · - · -), 5.5×10^{-3} s (— —), 6.2×10^{-3} s (- · · · · ·), 1.2×10^{-2} s (—o—).

Figure 4. Solvent and solute gaseous mass fractions versus the radial coordinate for NONA (80%)/DHBV(20%) clusters of uncharged (a) and charged (b) drops, The legend is the same as in Figs. 2 and 3.

Figure 5. Partial solvent and solute gaseous densities for NONA (80%)/DHBV(20%) clusters of uncharged (a) and charged (b) drops. The legend is the same as in Figs. 2 and 3.

Figure 6. Partial solvent and solute gaseous densities for NONA (80%)/QUAD(20%) clusters of uncharged (a) and charged (b) drops. Curves are for different times as follows: 6.8×10^{-5} s (· · · · ·), 7.5×10^{-4} s (—), 2.1×10^{-3} s (- - -), 3.5×10^{-3} s (- · - · -), 4.8×10^{-3} s (— —), 6.2×10^{-3} s (- · · · · ·), 1.2×10^{-2} s (—o—).

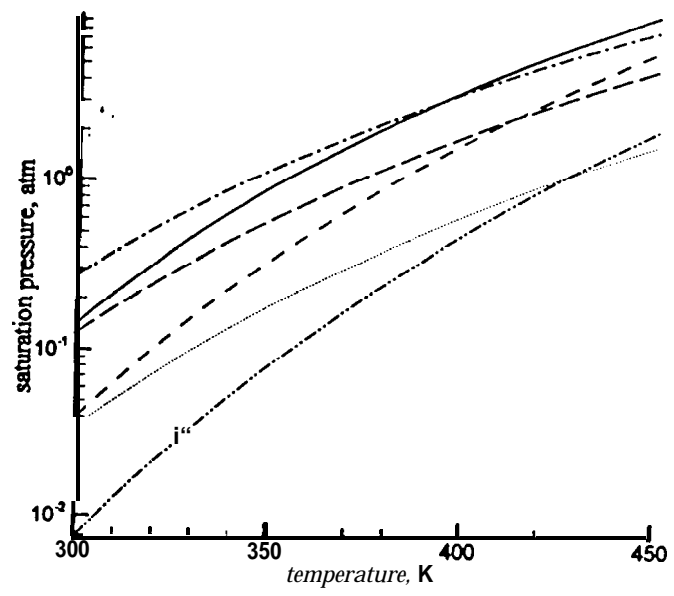


Fig. 1

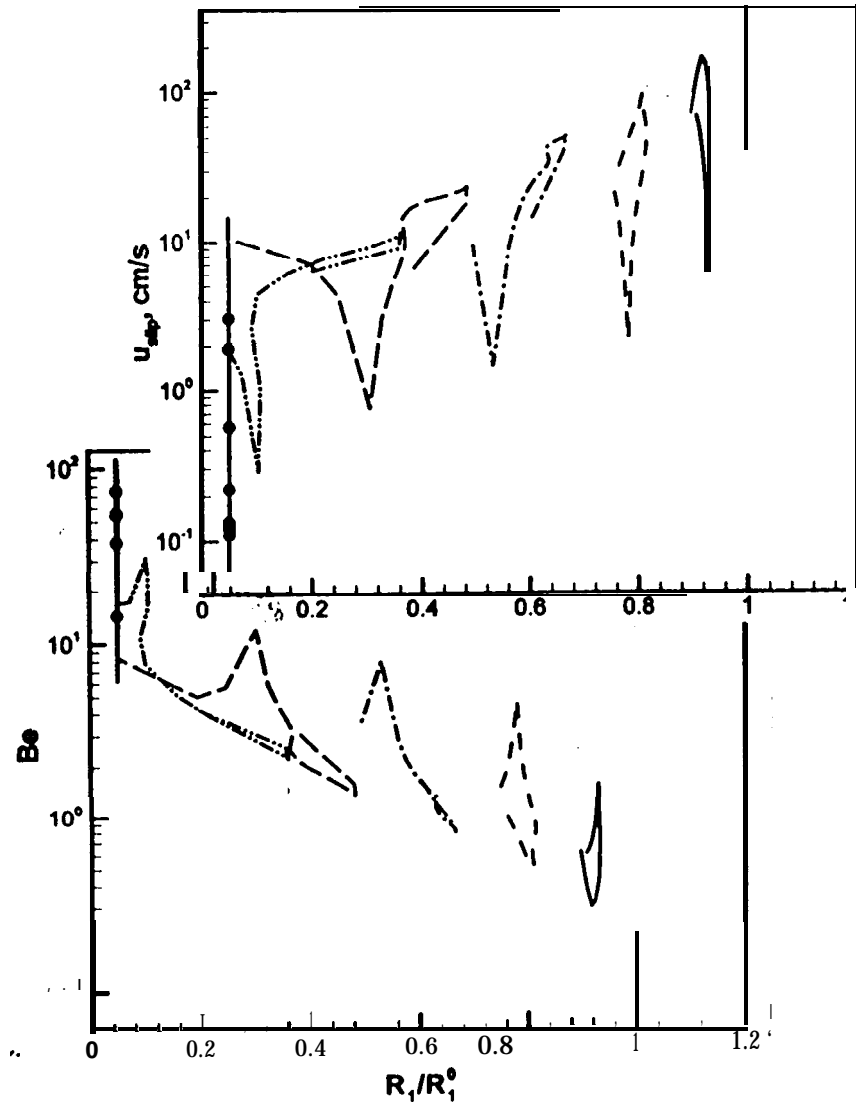


Fig 2a

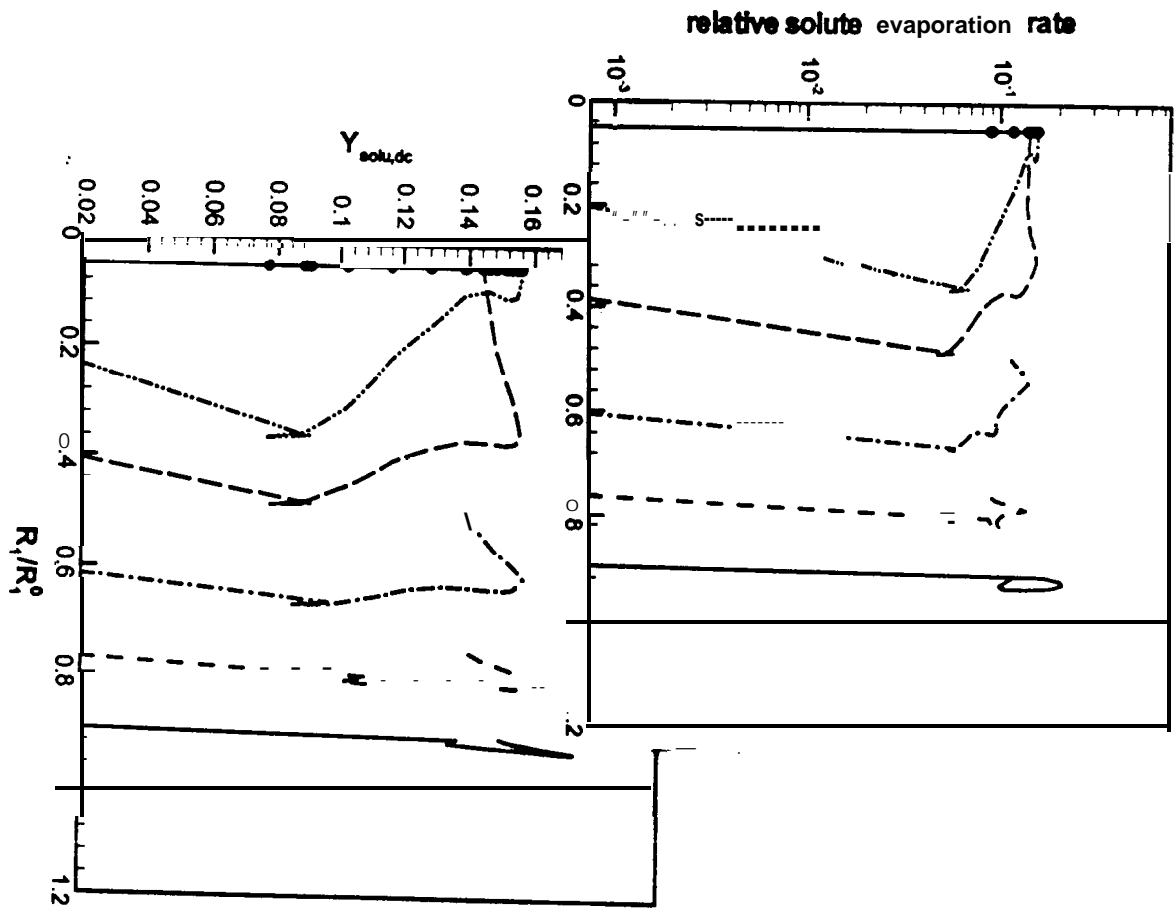


Fig. 26

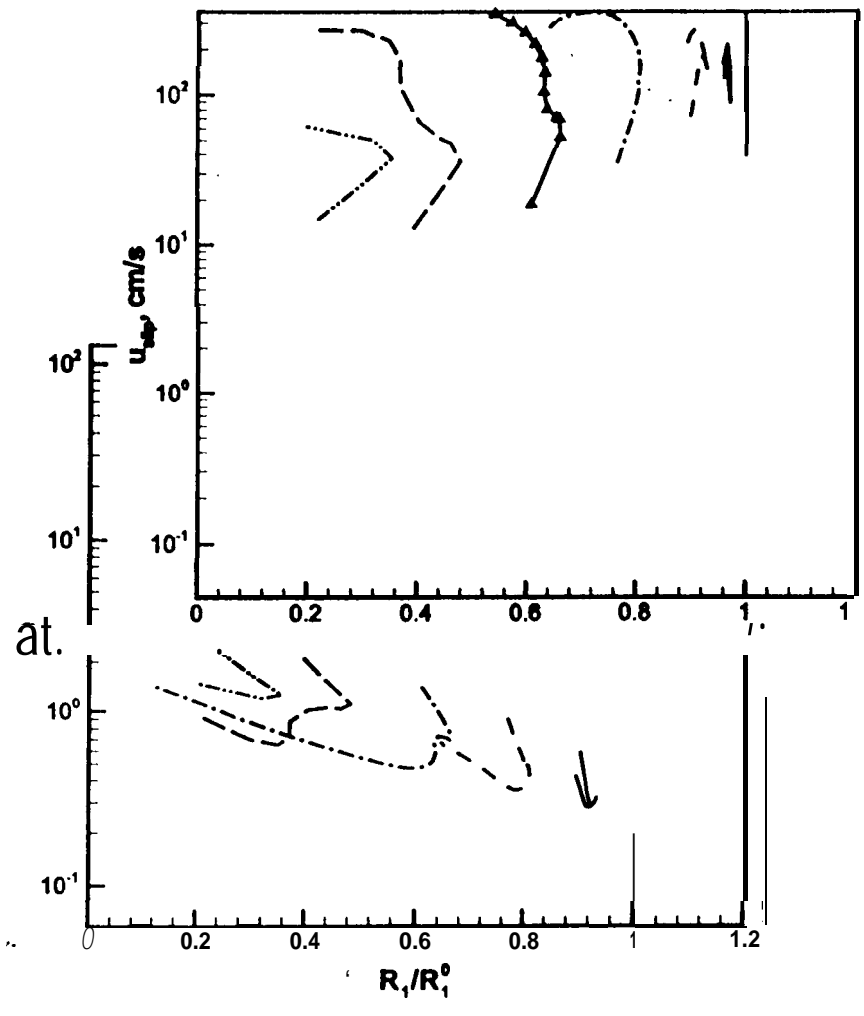


Fig 3a

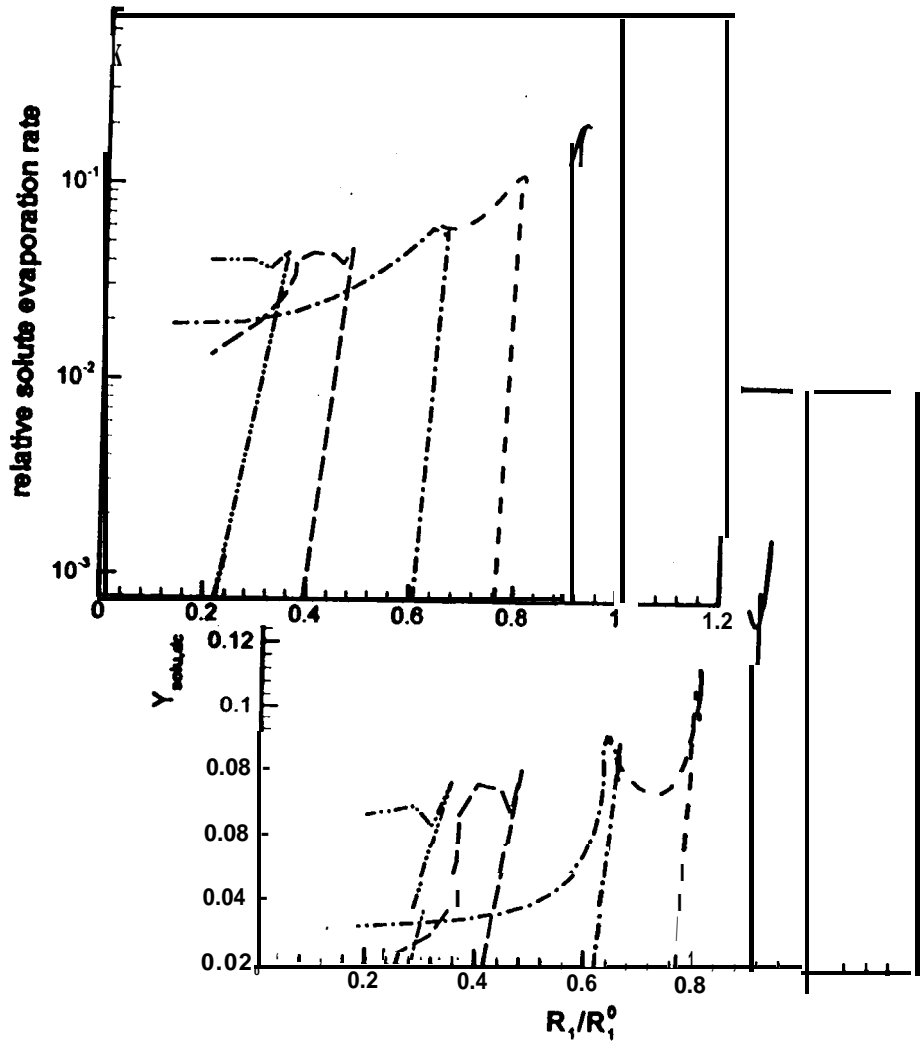


Fig 36

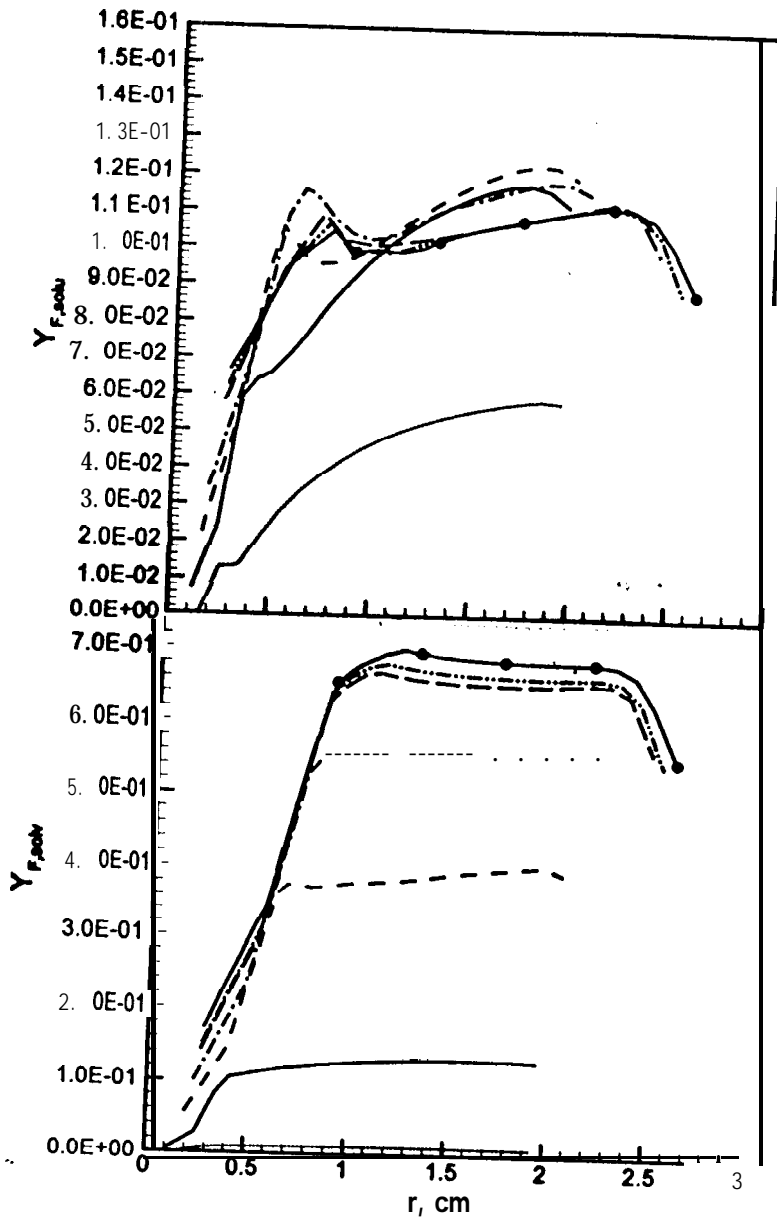


Fig 4a

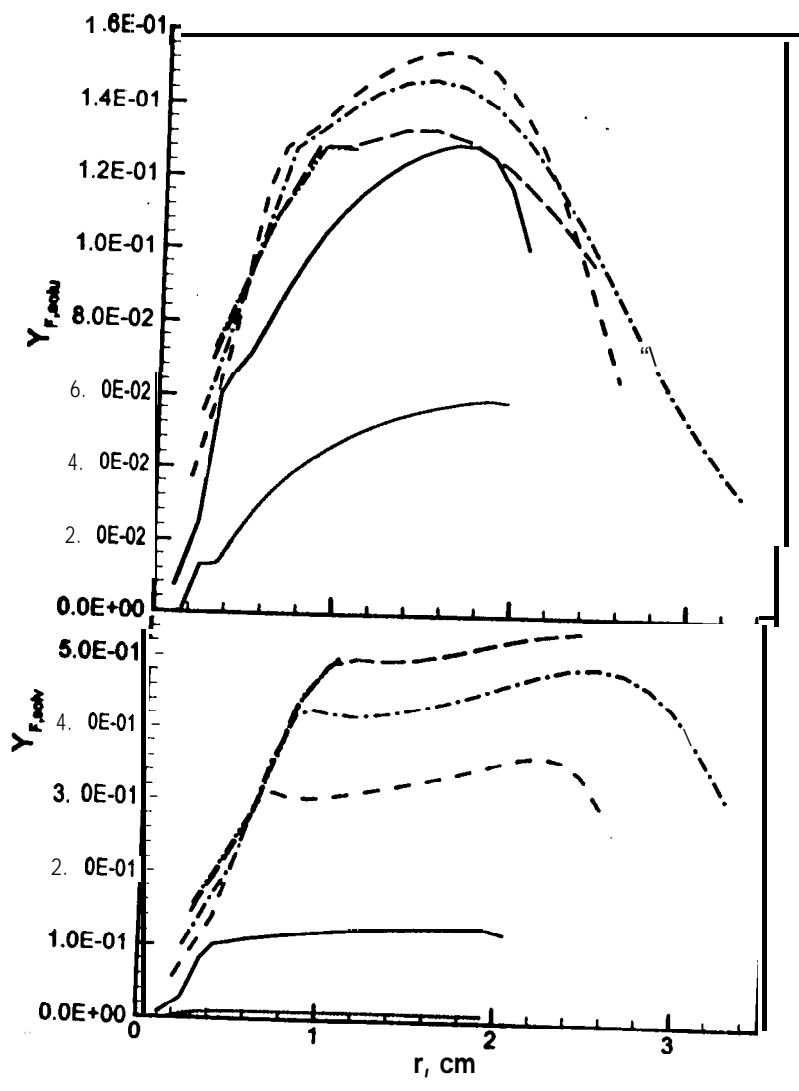


Fig 4b

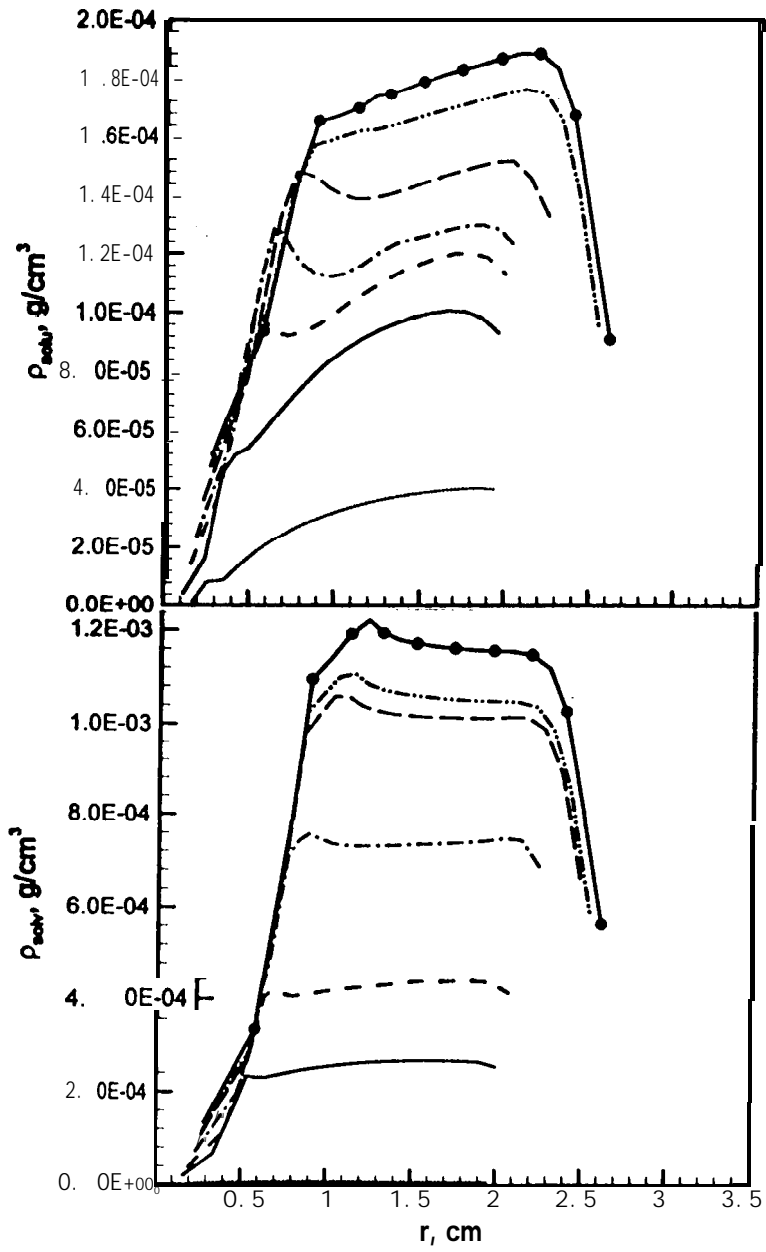


Fig 5a

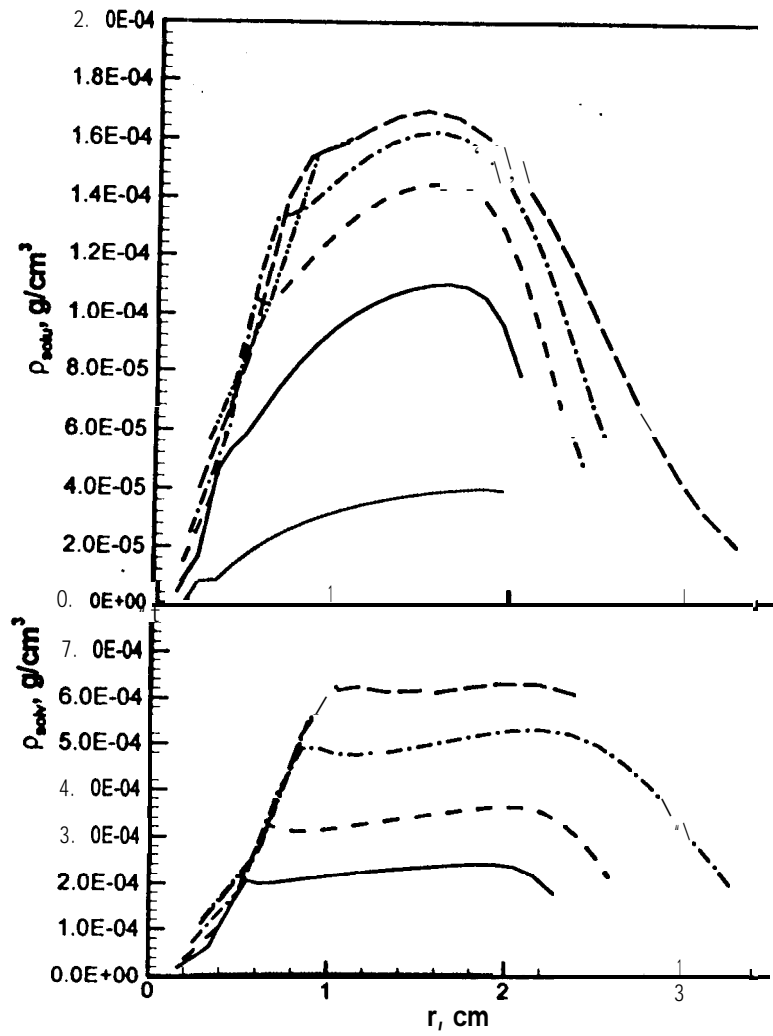


Fig 56

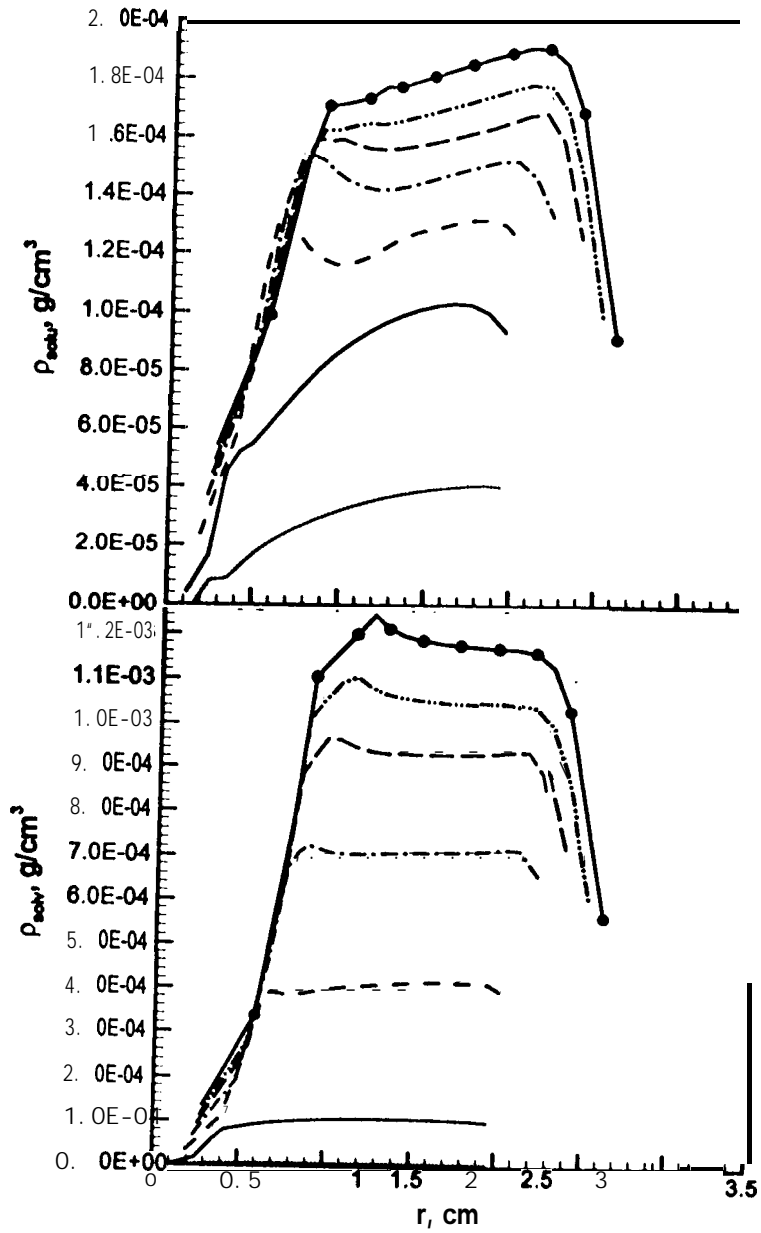


Fig 6a

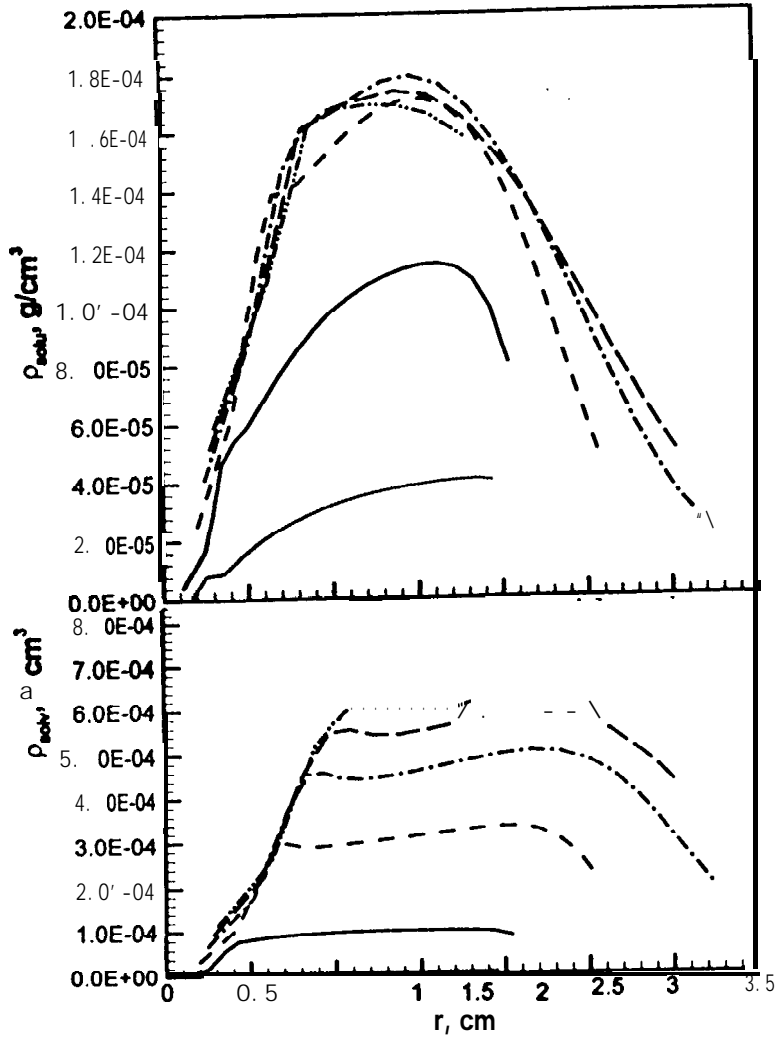


Fig 6b